RSC Advances

PAPER

View Article Online
View Journal | View Issue

Cite this: *RSC Adv.*, 2022, **12**, 19375

A novel, highly sensitive electrochemical 1,4-dioxane sensor based on reduced graphene oxide–curcumin nanocomposite†

Sana Fathima T. K.,[a] Arshiya Banu A.,[b] T. Devasena[b] and Sundara Ramaprabhu *[a]

Received 19th March 2022
Accepted 21st April 2022

DOI: 10.1039/d2ra01789j

rsc.li/rsc-advances

1,4-Dioxane is a carcinogenic, non-biodegradable, organic water pollutant which is used as a solvent in various industries. It is also formed as an undesired by-product in the cosmetic and pharmaceutical industry. Given its carcinogenicity and ability to pollute, it is desirable to develop a sensitive and selective sensor to detect it in drinking water and other water bodies. Current works on this sensor are very few and involve complex metal oxide composite systems. A sensitive electrochemical sensor for 1,4-dioxane was developed by modifying a glassy carbon electrode (GCE) with a reduced graphene oxide–curcumin (rGO–CM) nanocomposite synthesized by a simple solution approach. The prepared rGO–CM was characterized by X-ray Diffraction (XRD), Fourier Transform Infrared (FTIR) Spectroscopy, Raman spectroscopy, UV-Vis spectroscopy, and Scanning Electron Microscopy (SEM). The rGO–CM/GCE sensor was employed for the detection of 1,4-dioxane in the range of 0.1–100 μM. Although, the detection range is narrower compared to reported literature, the sensitivity obtained for the proposed sensor is far superior. Moreover, the limit of detection (0.13 μM) is lower than the dioxane detection target defined by the World Health Organization (0.56 μM). The proposed rGO–CM/GCE also showed excellent stability and good recovery values in real sample (tap water and drinking water) analysis.

1. Introduction

1,4-Dioxane is a non-biodegradable organic compound which is used as a solvent in various industrial processes such as the manufacture of resins, pharmaceuticals, oils, textiles, waxes, rubber chemicals *etc.* It is also obtained as an undesired by-product in the manufacture of ethylene oxide, ethylene glycol, and cosmetics.[1–3] It can be released into water bodies either accidentally or as a consequence of inefficient waste water treatment. Owing to its miscibility in water and hydrophilic nature, it can easily migrate through aquifers and cause widespread contamination of surface and ground waters. Additionally, the heterocyclic structure of the molecule with the two ether bonds renders it highly resistant to both biotic and biologically mediated degradation.[2] IARC (International Agency for Research on Cancer) has identified 1,4-dioxane as a probable human carcinogen (Group 2B). Thus, 1,4-dioxane contamination is a growing threat to the ecosystem and is harmful to animals and humans. The recent guidelines for drinking water quality issued by the World Health Organization (WHO) state a guideline value of 50 μg l^{-1} (0.56 μM) for 1,4-dioxane.[1]

In view of its carcinogenicity and ability to pollute, reliable detection of dioxane levels in water is necessary. Conventional analytical techniques for dioxane detection involve gas chromatography coupled mass spectrometry (GC-MS), GC-MS coupled with solvent extraction *etc.*[4,5] Although highly sensitive, these are expensive, time-consuming, and require sample preparation and trained personnel. In this context, it is desirable to devise a sensitive and selective electrochemical sensor to detect dioxane levels in drinking water and water bodies. Electrochemical sensing technique has the advantage of being highly sensitive and offers low detection limits. These can also be easily miniaturized for on-site testing. As compared to conventional techniques, this method does not require any sample extraction or pre-treatment, hence being suitable for real-time testing. So far, there have been only very few reports on electrochemical sensors for 1,4-dioxane.[3,6–8] These mainly involve complex metal oxide composites, which require time-consuming synthesis.

Curcumin is a hydrophobic polyphenolic pigment present in the rhizomes of *Curcuma longa* L., commonly known as turmeric.[9] It is also present in some other species of Curcuma, such as *Curcuma zedoaria*.[10] Turmeric is an essential component in the Indian system of medicine (Ayurveda) and is also commonly used as a spice and food preservative. Curcumin has numerous biological properties, which include antioxidant, antimicrobial, anti-carcinogenic, and anti-inflammatory

[a]*Alternative Energy and Nanotechnology Laboratory, Nano Functional Materials and Technology Centre (NFMTC), Department of Physics, Indian Institute of Technology Madras, Chennai 600036, India. E-mail: ramp@iitm.ac.in*

[b]*Centre for Nanoscience and Technology, A.C. Tech Campus, Anna University, Chennai 600025, India*

† Electronic supplementary information (ESI) available. See https://doi.org/10.1039/d2ra01789j

activities.[10–12] Recently, it was also found that it has high electrocatalytic activity towards toxic, carcinogenic analytes such as hydrazine, 4-nitrophenol, and methyl parathion.[9,13,14] The electrocatalytic property was attributed to the presence of *o*-methoxy phenolic groups in its structure.[13]

Graphene and its derivatives have been extensively used in electrochemical applications owing to its unique properties, such as two-dimensional crystalline sheet-like structure, high surface area, and high electrical conductivity.[15] Among them, reduced graphene oxide (rGO) has found tremendous application in sensors due to the ease of bulk synthesis compared to graphene. Electrodes modified with rGO were reported to have better electron transfer to the electrodes while simultaneously providing high surface area and functional groups for efficient analyte adsorption.[16] It is usually synthesized by reducing graphene oxide *via* chemical or electrochemical methods.[17] Hatamie S. *et al.*[18] reported green reduction and simultaneous functionalization of graphene oxide using curcumin as the reductant. By incorporating curcumin in the reduced graphene oxide structure, a composite with high effective surface area, better charge transfer, and proper functional groups (carbonyl, hydroxyl, carboxylic acid, and benzene rings) is created.[14,18]

In the present work, we have utilized a reduced graphene oxide–curcumin nanocomposite modified glassy carbon electrode (rGO–CM/GCE) as a sensitive electrochemical sensor for 1,4-dioxane. To the best of our knowledge, this is the first report on rGO–CM/GCE being employed for electrochemical detection of an analyte. The rGO–CM nanocomposite was synthesized *via* a facile approach, wherein the curcumin simultaneously reduced, exfoliated, and functionalized graphite oxide. The rGO promotes the electron transfer and provides a high surface area for the analyte adsorption, whereas the curcumin is selective to dioxane. We have also, for the first time, experimentally elucidated the possible sensing mechanism. The applicability of the proposed sensor in real water samples has also been demonstrated.

2. Materials and methods

2.1. Materials

Graphite (99.99% SP-1, Bay Carbon) with a particle size of 45 μm was used. Potassium permanganate ($KMnO_4$, 99.5%), sodium nitrate ($NaNO_3$, 99.5%), sodium chloride (NaCl, 99.99%), potassium dihydrogen phosphate (KH_2PO_4), potassium phosphate dibasic (K_2HPO_4) and concentrated sulphuric acid (H_2SO_4, 98%) were purchased from Rankem chemicals, India. Hydrogen peroxide (H_2O_2, 30%) was obtained from SD Fine-Chem Ltd. India. 1,4-Dioxane ($C_4H_8O_2$, 99%), potassium ferrocyanide ($K_4[Fe(CN)_6]$), potassium ferricyanide ($K_3[Fe(CN)_6]$), and curcumin ($C_{21}H_{20}O_6$) were obtained from SRL Pvt. Ltd. Nafion® solution was purchased from Sigma Aldrich. All chemicals were of analytical grade. Millipore deionized (DI) water (18 MΩ) was used to prepare all the solutions for synthesis and electrochemical characterizations.

2.2. Synthesis of graphite oxide (GO)

Graphite oxide (GO) was synthesized by the modified Hummer's method explained elsewhere.[17] In brief, 2 g of graphite was added to 46 ml of concentrated sulphuric acid under continuous stirring in a beaker on an ice bath. To this, 1 g of sodium nitrate and 6 g of potassium permanganate were added pinchwise simultaneously. Further, the ice bath was removed, and the solution was allowed to reach room temperature. Then, 92 ml of DI water was added dropwise and diluted further with 280 ml warm water. Further, a few ml of H_2O_2 was added. The solution was then added to 1 L water and allowed to settle. It was then filtered using 0.45 μm Whatman filter paper. The filtride was then washed several times with water, ethanol, and DI water successively. The washing was done until the pH changed to ~6. Further, the filtride was dried at 60 °C for 12 hours on a hot plate.

2.3. Synthesis of the reduced graphene oxide–curcumin (rGO–CM) nanocomposite

For the preparation of the reduced graphene oxide–curcumin nanocomposite (rGO–CM), equal amounts of the GO solution (3 mg ml^{-1} in DIW) and curcumin solution (2 mg ml^{-1} in ethanol) were sonicated for 15 minutes. The solution was then stirred using a magnetic stirrer for 12 h. Further, the rGO–CM nanocomposite was dried at 70 °C on a hot plate. To compare the sensing responses, samples were also prepared by varying the curcumin loading (0.05, 1, 3, 5 mg ml^{-1}).

2.4. Modification of the glassy carbon electrodes

Prior to deposition, the glassy carbon electrodes were thoroughly cleaned by polishing gently on nylon pads with alumina powder of diameters 1, 0.3, and 0.05 μm consecutively. It was further washed with DI water and ethanol. 5 mg of the prepared rGO–CM nanocomposite was sonicated in 50 μl ethanol. To it, 5 μl of Nafion (5 wt%) was added, which acts as a binder. 5 μl of this slurry was drop-casted on a glassy carbon electrode and dried at room temperature. The amount of ethanol–Nafion and the quantity to be deposited were optimized. For comparison, GO/GCE and curcumin/GCE (CM/GCE) were also fabricated in the same way.

2.5. Characterization

The structural, morphological, optical, and electrochemical properties of the synthesized powders were characterized using different techniques. The phase formation of the powders was confirmed using Powder X-ray Diffractometer (PANalytical X'Pert Pro XRD) with nickel filtered Cu K_α radiation in the 2θ range of 5° to 90° and a step size of 0.016°. The functional groups in the samples were identified by PerkinElmer Fourier Transform Infrared Spectroscopy (FTIR) in a wavenumber range of 4000–650 cm^{-1}. The UV-Vis absorption spectra of the samples and the dioxane oxidation product were obtained by Agilent Technologies Cary 100 UV-Visible Spectrophotometer. The defect and graphitic content information were obtained from the Raman spectra (Horiba Jobin Yvon LabRam HR800, 632 nm, 600 lines per mm grating, 30 s acquisition). The morphology of the samples was characterized by Scanning Electron Microscope (TESCAN VEGA3, 30 kV). The zeta potentials of the samples dispersed in deionized water were obtained

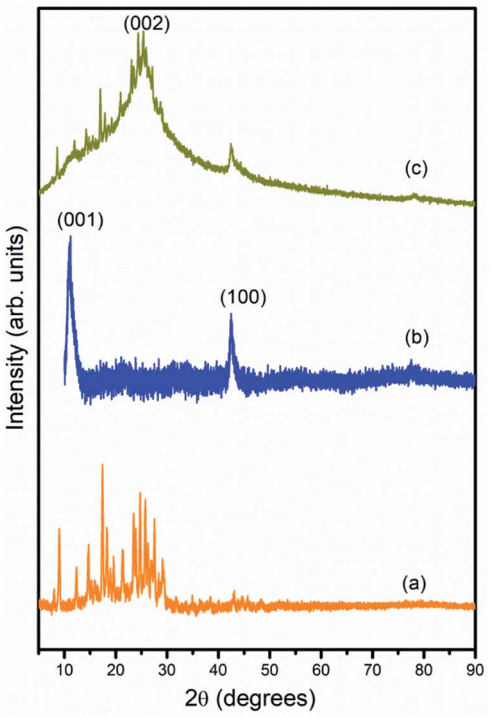

Fig. 1 X-ray diffraction patterns of (a) curcumin, (b) GO, and (c) rGO–CM.

by Malvern Instruments Ltd. All the electrochemical characterizations of the prepared sensors were carried out using CHI6083C Electrochemical Workstation. For the measurements, a conventional three-electrode system was employed with glassy carbon (3 mm diameter), Ag/AgCl (3 M KCl), and platinum wire electrodes as the working, reference, and counter electrodes, respectively.

3. Results and discussion

3.1. Physicochemical analysis of the prepared rGO–CM samples

3.1.1. X-ray diffraction. The XRD patterns of curcumin, GO, and rGO–CM are shown in Fig. 1. Pure curcumin exists in the crystalline state with well-defined sharp peaks in the 2θ range of 5–30°. The oxidation of graphite to graphite oxide results in the introduction of oxygen functional groups between the graphitic layers. This increases the interlayer spacing and shifts the 002 peak to lower 2θ values. This is observed in Fig. 1b, wherein the characteristic graphite peak shifts to ~11° corresponding to an interlayer spacing of 0.8 nm (indexed as 001 reflection).[17,19] For the rGO–CM sample (Fig. 1c), the 001 peak observed for GO is found to be shifted to ~10.4° with an interlayer spacing of 0.85 nm. This denotes the separation of the GO layers to form graphene oxide. Further, an intense, broad peak at 25.2°

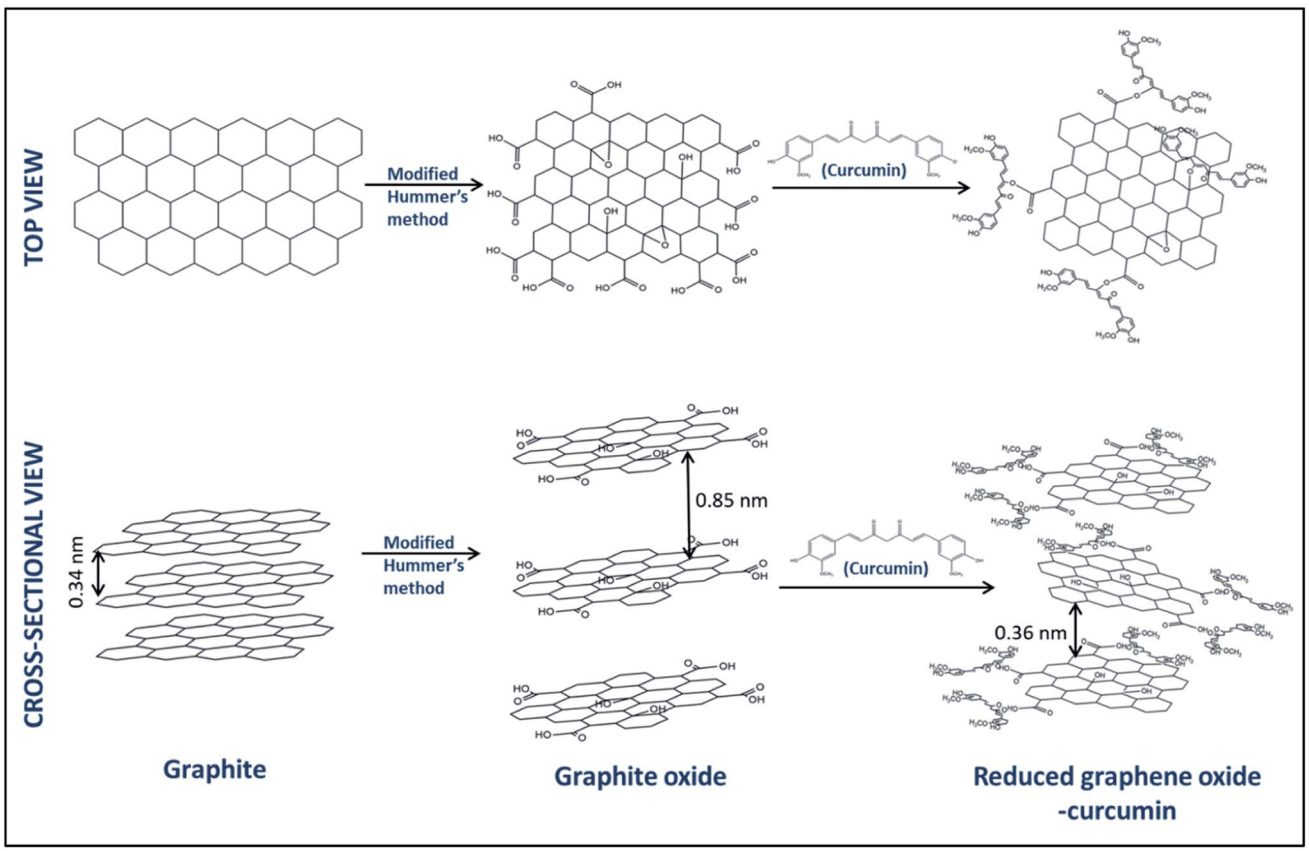

Fig. 2 Schematic representation of the changes in the graphite structure during the synthesis of the rGO–CM nanocomposite. The top and bottom rows indicate the top view and cross-sectional view respectively. The changes in interlayer distances are also depicted.

appears, corresponding to the 002 reflection of graphite and an interlayer spacing of 0.36 nm. This denotes the removal of the oxygen groups from the graphene oxide and subsequent formation of reduced graphene oxide (rGO).[18] The intensity of the 001 peak is very low, confirming that most of the graphene oxide has converted to rGO. The characteristic peaks of curcumin are also present overlaid on the rGO peak, albeit with lesser intensity than pure curcumin. This confirms the interaction between curcumin and rGO, and thereby the formation of the rGO–CM nanocomposite. The graphite oxide synthesized *via* the modified Hummer's approach undergoes simultaneous exfoliation, reduction, and functionalization during interaction with curcumin to form the rGO–CM nanocomposite. The synthesis process and the resultant products are elucidated in Fig. 2.

3.1.2. UV-vis spectroscopy. The presence of curcumin in the nanocomposite is further confirmed using UV-visible spectrophotometer. The spectra of rGO–CM, GO, and curcumin was recorded in ethanol (Fig. 3). The absorption peaks observed at 428 nm (strong), 265 nm (weak), and 207 nm (weak) are characteristic of curcumin. The maximum absorption is attributed to the electronic dipole allowed π–π* type excitation of its extended conjugation system.[20] For the graphite oxide, a strong absorption peak corresponding to the π–π* transitions of the aromatic C–C bonds is observed at 245 nm. A weak absorption shoulder corresponding to n–π* transitions of aromatic C=O bonds is also observed at 314 nm.[21] In the rGO–CM nanocomposite, absorption peaks of both the curcumin and GO are observed. This suggests that the chromophore group in curcumin is intact (diarylheptanoid) upon interaction with rGO, which is also helpful for sensing 1,4-dioxane.[18,22] Since the curcumin attaches to rGO *via* the π–π stacking mechanism, the delocalization of the π electrons decreases. This is seen by the shift of the absorption peaks of π electrons in rGO–CM towards the lower wavelength region.

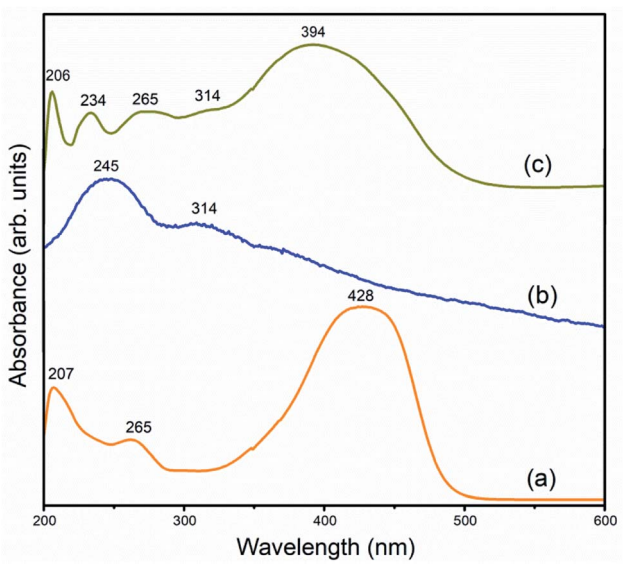

Fig. 3 UV-Vis spectra of (a) curcumin, (b) GO, and (c) rGO–CM.

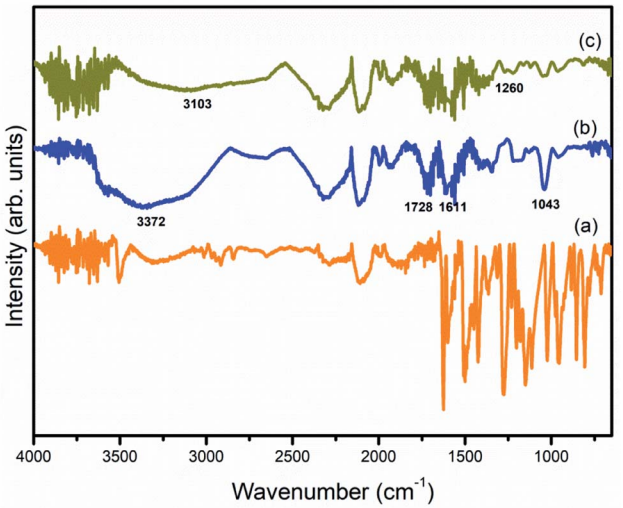

Fig. 4 FTIR spectra of (a) curcumin, (b) GO, and (c) rGO–CM.

3.1.3. Fourier-transform infrared (FTIR) spectroscopy. Fig. 4 depicts the FTIR spectra of curcumin, GO, and rGO–CM. The vibrations observed at 1728, 1043, 3372 cm^{-1} in GO are attributed to the oxygen-containing functional groups-carboxylic, epoxide, and hydroxyl groups, respectively. These peaks are found to be suppressed in rGO–CM, indicating the successful reduction of graphite oxide to rGO. The peak at 1611 cm^{-1} corresponds to the C=C vibration. The O–H stretching vibration peak in the rGO–CM (3103 cm^{-1}) is found to be shifted towards lower wavenumber as compared to GO (3372 cm^{-1}), which indicates the formation of hydrogen bonds in the former.[23,24] Therefore, the curcumin attachment to the reduced graphite oxide is due to a combination of both strong hydrogen bonds and π–π stacking. The characteristic C–O methyl bond of curcumin is also observed in the rGO–CM spectra in the range of 1260 cm^{-1}.[10,18]

3.1.4. Scanning electron microscope (SEM). The SEM images of GO and rGO–CM are shown in Fig. 5. GO exhibits flakes with a sheet-like morphology consisting of thin and wrinkled layers. In rGO–CM, the sheet-like morphology is maintained, with slight agglomeration or shortening of the flakes due to removal of oxygen functional groups and attachment of curcumin.[18,23]

3.1.5. Raman spectroscopy. The Raman spectra of the samples are shown in Fig. 6. The spectrum of curcumin shows many characteristic vibrations, which are explained elsewhere.[20] Graphite oxide and rGO–CM show two prominent peaks corresponding to the vibrations of the graphitic plane and the defects present in them. The peak observed at 1585 cm^{-1} corresponds to the graphitic (G) band arising due to the in-plane vibrations of the sp^2 hybridized carbon atoms. The one at 1338 cm^{-1} corresponds to the defect (D) band arising due to the presence of structural defects. The intensity ratios of D and G bands provide a measure of the defects on the graphitic structure.[17,20] The I_D/I_G ratio is calculated to be 1.158 and 1.337 for GO and rGO–CM, respectively. The increase in the ratio indicates the defects introduced during the curcumin-induced reduction of GO, and the attachment of curcumin to the graphitic structure.[18]

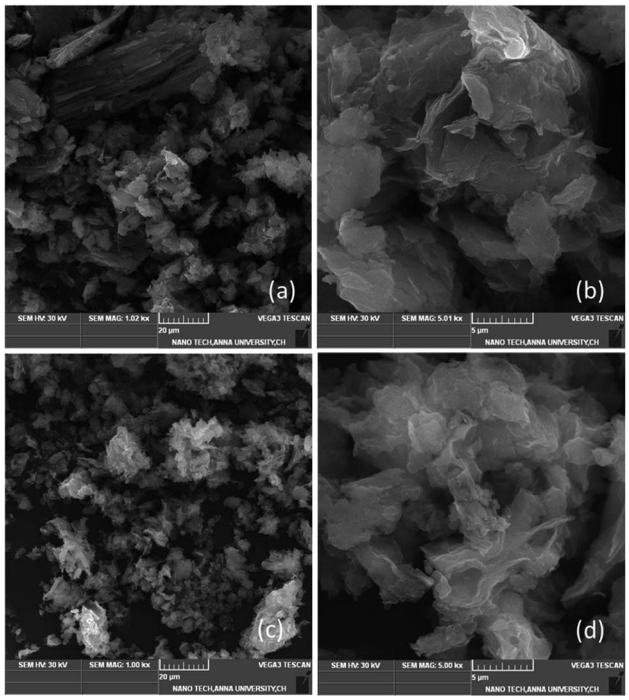

Fig. 5 SEM images of GO (a) 20 μM scale bar, (b) 5 μM scale bar and rGO–CM (c) 20 μM scale bar, (d) 5 μM scale bar.

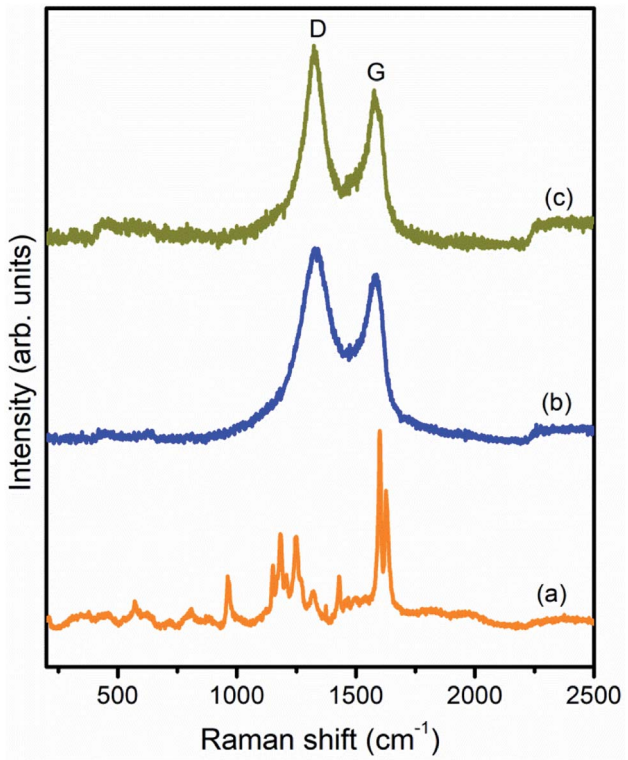

Fig. 6 Raman spectra of (a) curcumin, (b) GO, and (c) rGO–CM.

3.1.6. Zeta potential analysis. The zeta potentials of the GO and rGO–CM are found to be −19.5 and −3.06 mV, respectively. The potential distributions are illustrated in Fig. S3.† The larger negative value for GO implies the presence of more oxygen-containing functional groups in it.[25]

3.2. Electrochemical characterization of the prepared rGO–CM/GCE sensor

3.2.1. Electrochemical impedance spectroscopy (EIS). The electrochemical impedance measurement was carried out in a 1 : 1 mixture of 0.018 M PBS buffer and $K_3[Fe(CN)_6]$/$K_4[Fe(CN)_6]$ (1 : 1) in a frequency range of 0.01–10^5 Hz. The Nyquist plots of the various modified electrodes are shown in Fig. 7. The charge transfer resistance (R_{ct}) value indicates the electron transfer kinetics at the electrode/electrolyte interface. From the curves, the measured R_{ct} values for bare GCE, GO/GCE, CM/GCE, and rGO–CM/GCE are found to be 3649.6, 3416.96, 174.08, and 156 Ω, respectively. The lowest R_{ct} value is observed for rGO–CM/GCE, indicating better electron transfer and lower interface resistance than the other electrodes.

3.2.2. Linear sweep voltammetry. The electrochemical responses of the modified electrodes were studied by comparing their linear sweep voltammograms (0 to +1.5 V, 50 mV s^{-1}) in PBS (pH 7) containing 15 mM dioxane (Fig. 8). The highest current response at applied potential +1.5 V was observed for the rGO–CM electrode, indicating its better performance towards dioxane sensing. To compare the effect of the amount of curcumin in the composite, samples were prepared with different initial concentrations of curcumin (0.05, 1, 2, 3, 5 mg ml^{-1}). The XRD (Fig. S1†) and FTIR (Fig. S2†) patterns of the samples and their Nyquist, LSV plots (Fig. S4 and S5†) in 15 mM dioxane are depicted in the ESI section (S1 and S2†). It was found that a curcumin loading of 2 mg ml^{-1} was optimum to obtain the highest current under the present experimental conditions.

3.3. Analysis of sensing performance

In order to determine the sensing performance, the proposed sensor was utilized to sense different concentrations of dioxane

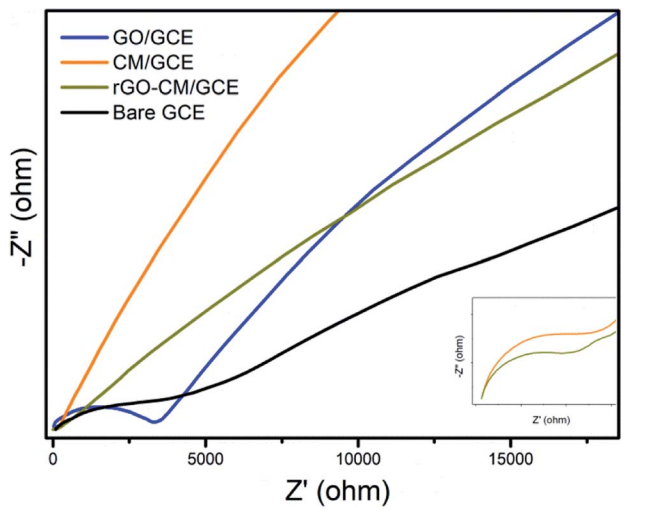

Fig. 7 Nyquist plots of bare GCE, GO/GCE, CM/GCE, and rGO–CM/GCE. The semicircle region of CM/GCE and rGO–CM/GCE is shown in the inset.

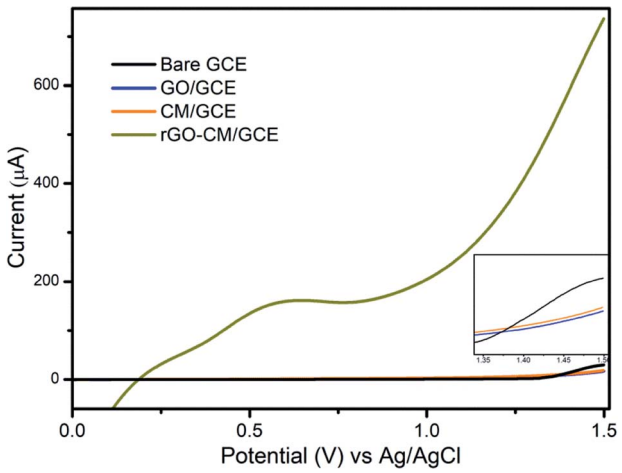

Fig. 8 Linear sweep voltammograms of bare GCE, GO/GCE, CM/GCE, and rGO–CM/GCE in 15 mM 1,4-dioxane solution. Inset shows the zoomed-in portion near 1.5 V.

(6–126 μM). Before analyte addition, the current responses of the modified electrodes were stabilized in PBS solution (25 ml, pH 7). Further, 10 μl aliquots of 15 mM 1,4-dioxane stock solution were serially added to the solution. The solution was stirred thoroughly after each addition. After each addition, a linear sweep voltammogram was recorded with a scan rate of 0.05 V s^{-1} in the potential range from 0 to +1.5 V. The electrode was gently washed with PBS solution before each measurement. The current responses are depicted in Fig. 9. It was observed that the current increased with each addition of dioxane. Interestingly, it was noted that in contrast to previous reports,[3,5,6] we observed a linear relation for the current with concentration rather than with the logarithm of concentration. The corresponding calibration curve, plotted with the current at +1.5 V *versus* the applied potential, is illustrated in Fig. 9b–d. Two linear regions are observed in the curve; 6–54 μM and 60–102 μM with linear regression equations $I\,(\mu A) = 0.33033C\,(\mu M) + 22.88$ and $I\,(\mu A) = 0.667C\,(\mu M) + 3.878$ respectively. The sensitivities for each linear range was calculated as the ratio of observed slope to the electrode area (0.0707 cm^{-2}) and were found to be 4.67 μA μM^{-1} cm^{-2} for 6–54 μM, and 9.445 μA μM^{-1} cm^{-2} for 60–102 μM. The sensing experiment was repeated thrice to confirm the detection range. To further lower the detection limit, the experiment was repeated with 5 mM dioxane stock solution. The observed linear sweep voltammogram and the corresponding current response at +1.5 V are

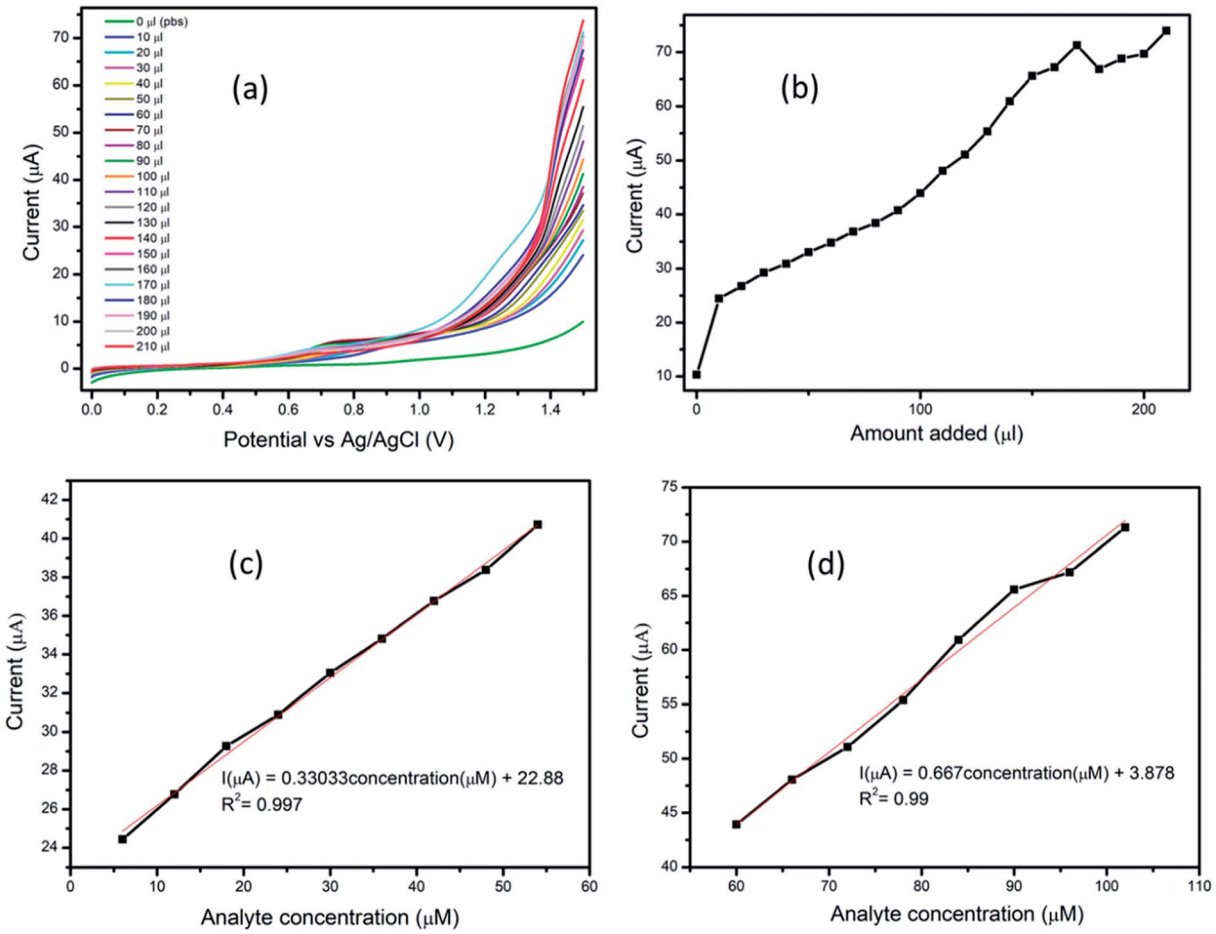

Fig. 9 (a) Linear sweep voltammograms of rGO–CM/GCE in increasing concentration (6–105 μM) of 1,4-dioxane and (b) its corresponding calibration curve. The two linear regions are separately shown in (c) and (d), with the red line indicating the best linear fit.

illustrated in Fig. S8.† A linear detection range of 1–10 μM with a linear regression equation of I (μA) = 1.369C (μM) + 34.11 and a high sensitivity of 19.36 μA μM^{-1} cm^{-2} was observed. In order to achieve detection at the WHO guideline value, the experiment was performed by adding 50 μl aliquots of 50 μM dioxane stock solution to 25 ml PBS. As observed in the corresponding linear sweep voltammograms and calibration curve (Fig. S9†), two linear regions are present: 0.1–0.3 μM with a linear regression equation of I (μA) = 10.1C (μM) + 12.22 and 0.4–0.9 μM with a linear regression equation of I (μA) = 3.44C (μM) + 16.44. The sensitivities are 142.8 μA μM^{-1} cm^{-2} and 48.65 μA μM^{-1} cm^{-2} respectively. The limit of detection and limit of quantification were calculated as

$$\mathrm{LOD} = \frac{3.3\sigma}{S} \quad (1)$$

$$\mathrm{LOQ} = \frac{10\sigma}{S} \quad (2)$$

where σ is the standard deviation of the y-intercept and S is the slope of the calibration curve.

The LOD and LOQ were found to be 0.13 μM and 0.39 μM, respectively.

3.4. Possible sensing mechanism

Previous reports on 1,4-dioxane sensors proposed different oxidation mechanisms. Some involved oxidation of 1,4-dioxane to formic acid and oxalic acid,[3,7] whereas one involved its oxidation to carbon dioxide and hydrogen gas on reaction with water in the buffer solution.[6] Chitra S. *et al.*[26] reported the formation of acidic intermediates during the degradation of dioxane based on the change in pH. Zeng *et al.*[27] identified formic acid as the primary oxidation product of dioxane, with other acids such as oxalic acid, acetic acid, methoxyacetic acid, *etc.*, as the minor products. In the present report, the dioxane solution after the sensing experiment was subjected to a UV-Vis spectroscopy study to investigate the oxidation mechanism.

1,4-Dioxane is a Lewis base, having electron-donor abilities towards electron acceptors such as aromatic rings.[22] It has been reported that 1,4-dioxane can undergo oxidation in pH 7 under appropriate potential.[3] The presence of curcumin, with the electron-withdrawing methoxy group, facilitates the oxidation of dioxane. An insight into the interaction between dioxane and curcumin can be obtained from their UV-Vis spectra (Fig. S6†). Initially, the spectrum was obtained for the reduced graphene oxide–curcumin composite dispersed in ethanol. Further, the spectrum was measured after addition of a specific amount of dioxane (15 mM). As seen from Fig. S6,† the characteristic peak of curcumin 425 nm is found to be suppressed with increasing dioxane concentration in the solution. This may indicate the attachment of dioxane to the curcumin, specifically at the chromophoric group, hence reducing its absorption intensity. The presence of curcumin thereby increases the affinity of the dioxane molecules towards the rGO–CM/GCE.

The confirmation of the oxidation products was also done using UV-Vis spectroscopy (Fig. S7†). An absorption peak at 193 nm is observed for the dioxane solution after the electrochemical sensing experiment. A similar peak is obtained for dioxane solution mixed with a few ml of formic acid. This confirms the major presence of formic acid in the post-oxidation solution. Going by reported literature,[27] the minor product may be oxalic acid. The electrons lost during the oxidation process enhance the conductivity of the sensing medium. The electrochemical response hence increases with increasing dioxane concentration. The mechanism is summarized in Fig. 10.

3.5. Selectivity test

To assess the selectivity of the proposed sensor towards 1,4-dioxane, LSV was performed in PBS containing interferants

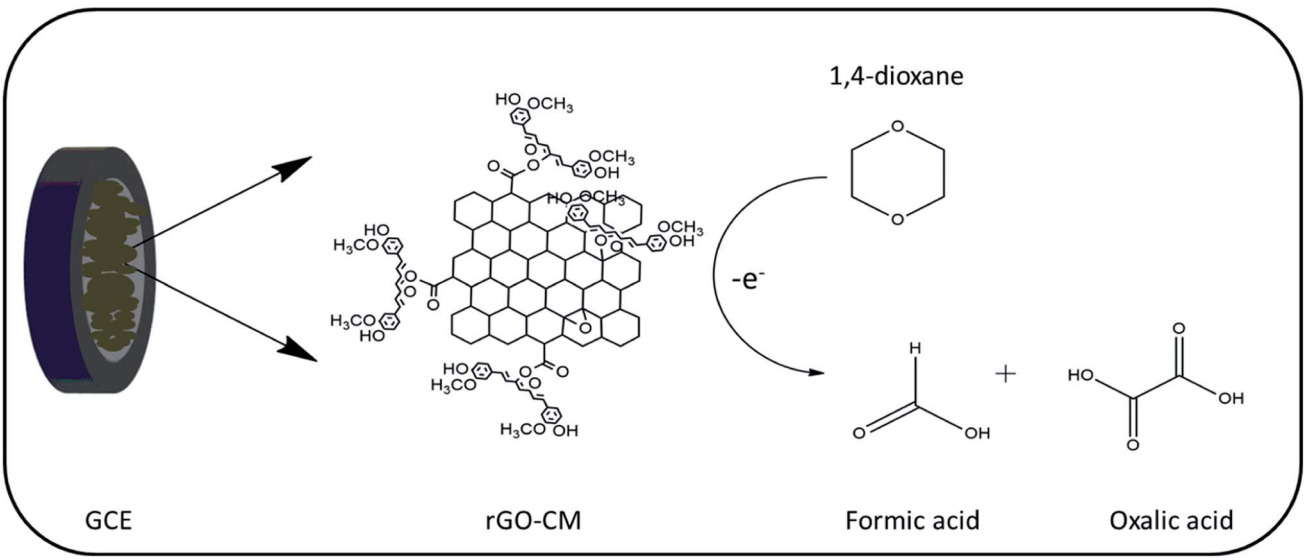

Fig. 10 Proposed reaction mechanism for 1,4-dioxane oxidation.

Table 1 Analysis of 1,4-dioxane in real samples using rGO–CM/GCE

Sample	Added 1,4-dioxane concentration (μM)	Measured 1,4-dioxane concentration using rGO–CM/GCE (μM)	Recovery (%)
Drinking water	60	61.34	102.2
Tap water	60	70.95	118.25

such as chlorobenzene, acetonitrile, and ethylene glycol (each of 15 mM concentration) (Fig. S10†) and the current at +1.5 V was compared. It can be observed that the highest current response was observed for 1,4-dioxane, indicating that the proposed rGO–CM/GCE sensor is more selective to 1,4-dioxane compared to other interferants.

3.7. Stability and reliability

Stability and reliability are essential parameters to assess the performance of a sensor. The proposed rGO–CM/GCE sensor was tested for its reliability by consecutively running seven LSV runs in dioxane solution (Fig. S11†). It was observed that the current at +1.5 V decreased slightly with each run. This may be due to the oxidation products getting adsorbed onto the electrode, thereby blocking the active sites for new dioxane molecules. A relative standard deviation (RSD) of 6.9% was observed for this measurement. The stability of the current response of the rGO–CM/GCE in 15 mM dioxane on different days was also analyzed. The result is shown in Fig. S12.† A slight decrease in current with an acceptable RSD of 12.4% ($n = 4$) was observed.

3.8. Repeatability

The repeatability of the rGO–CM/GCE sensor performance with different glassy carbon electrodes under identical experimental conditions was also analyzed. Fig. S13† shows the LSV results for the same. Similar current responses (RSD = 7%, $n = 3$) are observed for all the electrodes implying that the proposed sensor possesses good repeatability.

3.9. Real sample analysis

1,4-Dioxane is a common water pollutant, which is harmful for animals and humans. Therefore, the rGO–CM/GCE sensor was employed to detect dioxane in tap water and drinking water to demonstrate its applicability in real samples. The electrodes were initially stabilized in PBS before the real sample measurement. The water samples were then spiked with specific concentrations of dioxane, and recovery survey was performed. The spiked and calculated concentrations of dioxane are given in Table 1. The results reveal that the proposed rGO–CM/GCE sensor is suitable for the detection of 1,4-dioxane in real water samples.

4. Conclusion

Herein, a reduced graphene oxide–curcumin (rGO–CM) nanocomposite modified glassy carbon electrode has been successfully employed for the electrochemical detection of 1,4-dioxane. The rGO–CM nanocomposite was synthesized from graphite oxide by a simple approach using environment-friendly curcumin. Although the proposed sensor has a narrower linear range compared to reported literature, the sensitivity obtained is far superior. A comparison of the analytical parameters of the present study and reported literature is given in Table S1.† The limit of detection achieved, 0.13 μM, is lower than the WHO detection target of 0.56 μM. Formic acid was identified as the primary oxidation product of 1,4-dioxane under the present experimental conditions. The rGO–CM/GCE also showed appreciable selectivity, repeatability, stability, and excellent recovery in real sample analysis.

Conflicts of interest

There are no conflicts to declare.

Acknowledgements

Authors acknowledge the Indian Institute of Technology Madras (IITM), India, and the Ministry of Human Resources and Development, Government of India, for financial support. One of the authors thanks the Department of Science and Technology (DST) for the financial support to establish the Nano Functional Materials Technology Centre (NFMTC) through SR/NM/NAT/02-2005 project.

References

1 Y. Sayato, *Eisei Kagaku*, 1989, **35**, 307–312.
2 K. J. Godri, J. Kim, J. Peccia, M. Elimelech, Y. Zhang, G. Charkoftaki, B. Hodges, I. Zucker, H. Huang, N. C. Deziel, K. Murphy, M. Ishii, C. H. Johnson, A. Boissevain, E. O. Keefe, P. T. Anastas, D. Orlicky, D. C. Thompson and V. Vasiliou, *Sci. Total Environ.*, 2019, **690**, 853–866.
3 M. R. Karim, M. M. Alam, M. O. Aijaz, A. M. Asiri, M. A. Dar and M. M. Rahman, *Talanta*, 2019, **193**, 64–69.
4 P. E. Grimmett and J. W. Munch, *J. Chromatogr. Sci.*, 2009, **47**, 31–39.
5 M. M. Alam, A. M. Asiri, J. Uddin and M. M. Rahman, *J. Mater. Sci. Mater. Electron.*, 2022, **33**, 4360–4374.
6 M. M. Rahman, A. Wahid and A. M. Asiri, *New J. Chem.*, 2019, **43**, 17395–17402.
7 M. M. Rahman, M. M. Alam and A. M. Asiri, *RSC Adv.*, 2019, **9**, 42050–42061.
8 J. De Clercq, E. Van De Steene, K. Verbeken and M. Verhaege, *J. Chem. Technol. Biotechnol.*, 2010, **85**, 1162–1167.
9 B. Dinesh and R. Saraswathi, *Sensor. Actuator. B Chem.*, 2017, **253**, 502–512.

10 G. K. Athira and A. N. Jyothi, *Int. J. Pharm. Pharm. Sci.*, 2014, **6**(10), 171–176.
11 D. Zhang, X. Ouyang, J. Ma, L. Li and Y. Zhang, *Electroanalysis*, 2016, **28**, 749–756.
12 K. Li, Y. Li, L. Yang, L. Wang and B. Ye, *Anal. Methods*, 2014, **6**, 7801–7808.
13 L. Zheng and J. Song, *Sensor. Actuator. B Chem.*, 2009, **135**, 650–655.
14 A. Mejri, A. Mars, H. Elfil and A. H. Hamzaoui, *Microchim. Acta*, 2019, **186**, 704.
15 M. Tahriri, M. Del Monico, A. Moghanian, M. Tavakkoli Yaraki, R. Torres, A. Yadegari and L. Tayebi, *Mater. Sci. Eng. C*, 2019, **102**, 171–185.
16 H. Zhang, L. Cheng, H. Shang, W. Zhang and A. Zhang, *Russ. J. Electrochem.*, 2021, **57**, 872–884.
17 P. Divya and S. Ramaprabhu, *Phys. Chem. Chem. Phys.*, 2014, **16**, 26725–26729.
18 S. Hatamie, O. Akhavan, S. K. Sadrnezhaad, M. M. Ahadian, M. M. Shirolkar and H. Q. Wang, *Mater. Sci. Eng. C*, 2015, **55**, 482–489.
19 P. Chen, H. Li, S. Song, X. Weng, D. He and Y. Zhao, *Results Phys.*, 2017, **7**, 2281–2288.
20 H. Van Nong, L. X. Hung, P. N. Thang, V. D. Chinh, L. Van Vu and P. T. Dung, *Springerplus*, 2016, **5**, 1147.
21 D. Khalili, *New J. Chem.*, 2016, **40**, 2547–2553.
22 A. K. Nain, N. Chaudhary, Ankita, J. Gupta and P. Chandra, *J. Chem. Thermodyn.*, 2017, **108**, 145–161.
23 B. Kianpour, Z. Salehi and S. Fatemi, *Sci. Iran. C*, 2018, **25**, 1384–1394.
24 J. Joseph and E. D. Jemmis, *J. Am. Chem. Soc.*, 2007, **129**, 4620–4632.
25 B. Konkena and S. Vasudevan, *J. Phys. Chem. Lett.*, 2012, **3**, 867–872.
26 S. Chitra, K. Paramasivan, M. Cheralathan and P. K. Sinha, *Environ. Sci. Pollut. Res.*, 2012, **19**, 871–878.
27 Q. Zeng, H. Dong, X. Wang, T. Yu and W. Cui, *J. Hazard. Mater.*, 2017, **331**, 88–98.